© 2016. Published by The Company of Biologists Ltd | Journal of Cell Science (2016) 129, 1391-1403 doi:10.1242/jcs.177592

RESEARCH ARTICLE

Integrins synergise to induce expression of the MRTF-A–SRF target gene ISG15 for promoting cancer cell invasion

Michaela-Rosemarie Hermann[1,*], Madis Jakobson[1,*], Georgina P. Colo[1,*], Emanuel Rognoni[1], Maili Jakobson[1], Christian Kupatt[2], Guido Posern[3] and Reinhard Fässler[1,‡]

ABSTRACT

Integrin-mediated activation of small GTPases induces the polymerisation of G-actin into various actin structures and the release of the transcriptional co-activator MRTF from G-actin. Here we report that pan-integrin-null fibroblasts seeded on fibronectin and expressing β1- and/or αV-class integrin contained different G-actin pools, nuclear MRTF-A (also known as MKL1 or MAL) levels and MRTF-A–SRF activities. The nuclear MRTF-A levels and activities were highest in cells expressing both integrin classes, lower in cells expressing β1 integrins and lowest in cells expressing the αV integrins. Quantitative proteomics and transcriptomics analyses linked the differential MRTF-A activities to the expression of the ubiquitin-like modifier interferon-stimulated gene 15 (ISG15), which is known to modify focal adhesion and cytoskeletal proteins. The malignant breast cancer cell line MDA-MB-231 expressed high levels of β1 integrins, ISG15 and ISGylated proteins, which promoted invasive properties, whereas non-invasive MDA-MB-468 and MCF-7 cell lines expressed low levels of β1 integrins, ISG15 and ISGylated proteins. Our findings suggest that integrin-adhesion-induced MRTF-A–SRF activation and ISG15 expression constitute a newly discovered signalling circuit that promotes cell migration and invasion.

KEY WORDS: Cell migration, Integrin, ISG15, MRTF-A, SRF

INTRODUCTION

Integrin-mediated cell adhesion and signalling control numerous cellular processes, which are crucial for development and postnatal homeostasis, and influence diverse pathological processes such as cancer development and metastasis (Hynes, 2002; Winograd-Katz et al., 2014). Integrin signalling is a multistep process that is initiated with integrin activation and ligand binding, followed by integrin clustering and the progressive assembly of signalling platforms consisting of adaptor, signalling and/or catalytic and cytoskeletal proteins (Legate et al., 2009). The first integrin-based adhesion sites are small and short-lived and termed nascent adhesions. They eventually mature into large and stable focal adhesions that are connected to filamentous (F-) actin (Vicente-Manzanares et al., 2009).

Integrin signalling induces both short- and long-term effects in cells (Legate et al., 2009). The short-term effects mainly affect cytoskeletal rearrangements that allow cells to adopt their characteristic shape and initiate migration, and are to a large extent triggered by the activation of Rho family GTPases and actin-binding proteins (Danen et al., 2002). Long-term effects of integrin signalling result from changes in gene expression, which regulate numerous cellular processes including proliferation and differentiation (Legate et al., 2009). Integrin-dependent regulation of gene expression is primarily thought to arise from cross talk with growth factor receptors that increase the activity of mitogen-activated protein (MAP) kinase pathways. A recent study, however, reported that integrins can also control gene transcription by releasing the association of the transcriptional co-activator myocardin-related transcription factor-A (MRTF-A, also known as MKL1 or MAL) from monomeric or globular (G-) actin (Miralles et al., 2003; Plessner et al., 2015). MRTF-A belongs to the myocardin-related family of transcriptional co-activators, which consists of myocardin, MRTF-A and MRTF-B (also known as MKL2). MRTF-A and MRTF-B can bind monomeric G-actin, which retains them in the cytoplasm and prevents binding to SRF. Once G-actin is polymerised into different actin networks, MRTF-A/B are released from cytoplasmic and nuclear G-actin, associate with the transcription factor serum response factor (SRF) and regulate the expression of cytoskeletal proteins including actin and numerous focal adhesion proteins (Esnault et al., 2014; Posern and Treisman, 2006).

In the present paper we investigated whether fibronectin-binding integrins of the αV and β1 classes can regulate MRTF–SRF activity. To this end we used integrin-deficient fibroblasts (pan-knockouts, pKO cells) that were reconstituted with αV and/or β1 integrin cDNAs, giving rise to cells that express αVβ3 and αVβ5 (pKO-αV cells), cells that express α5β1 (pKO-β1), and cells that express both integrin classes (pKO-αV,β1 cells). We have shown in a previous paper that reconstituting cells with different fibronectin-binding integrins results in the formation of different types of adhesion sites and the induction of different actin structures (Schiller et al., 2013). Whereas the pKO-αV cells form large focal adhesions and primarily activate Rho–mDia-mediated actin polymerisation leading to thick, transversal stress fibres, pKO-β1 cells assemble small nascent adhesions along the cell edge, activate Rac, induce dense cortical actin networks and lamellipodia and link Rho primarily to myosin II activation. pKO-αV,β1 cells develop nascent adhesions, a cortical actin network at the cell edge and lamellipodia, and focal adhesions associated with stress fibres and high myosin II activity (Schiller et al., 2013). Using these cell lines we demonstrate that αV- and β1-class integrins synergise to induce high activation of MRTF–SRF and expression of target genes. We also identify the ubiquitin-like modifier interferon-stimulated gene 15 (ISG15) as a newly discovered integrin-induced MRTF–SRF target gene, and find that high levels of fibronectin-binding integrins and ISG15 promote the invasion of the malignant breast cancer line

[1]Department of Molecular Medicine, Max Planck Institute of Biochemistry, Martinsried 82152, Germany. [2]Medical Department, Cardiology, Klinikum rechts der Isar-Technische Universität München, Munich 81675, Germany. [3]Institute of Physiological Chemistry, Halle 06114, Germany.
*These authors contributed equally to this work

‡Author for correspondence (faessler@biochem.mpg.de)

Received 15 July 2015; Accepted 27 January 2016

Journal of Cell Science (2016) 129, 1391-1403 doi:10.1242/jcs.177592

MDA-MB-231 and correlate with poor survival rates in a large cohort of breast cancer patients.

RESULTS

Fibronectin-binding integrins differentially regulate actin distribution and ratios of G- and F-actin

To assess whether fibronectin-binding integrins differentially regulate MRTF-A–SRF activity, we seeded pKO-αV, pKO-β1 and pKO-αV,β1 cells (Schiller et al., 2013) on fibronectin and analysed the levels and distribution of MRTF-A, G-actin and F-actin. Western blots of whole cell lysates revealed significantly higher levels of β-actin in pKO-αV cells compared with pKO-β1 and pKO-αV,β1 cells (Fig. 1A,B), and staining with fluorescently labelled phalloidin showed that pKO-αV and pKO-αV,β1 cells developed thick stress fibres, whereas pKO-β1 contained thin stress fibres on fibronectin-coated culture dishes and micropatterns (Fig. 1C; Fig. S1A). Furthermore, pKO-β1 and pKO-αV,β1 cells formed multiple lamellipodia with subcortical actin networks, which were rarely seen in pKO-αV cells (Fig. 1C). Visualisation of cytoplasmic G-actin with fluorescently labelled DNaseI revealed high cytoplasmic signals in pKO-αV and lower signals in pKO-β1 and pKO-αV,β1 cells (Fig. 1D). To quantify the G- and F-actin levels in our cell lines, we performed cell fractionation assays followed by western blotting and found that the soluble fractions (G, containing G-actin and positive for GAPDH) contained higher β-actin levels in pKO-αV cells compared with pKO-β1 and pKO-αV,β1 cells (Fig. 1E), whereas the cytoskeletal fractions (F, containing F-actin and positive for Vimentin) contained highest β-actin levels in pKO-αV,β1, intermediate in pKO-β1 and lowest in pKO-αV cells (Fig. 1E). The calculated G-/F-actin ratio from nine different

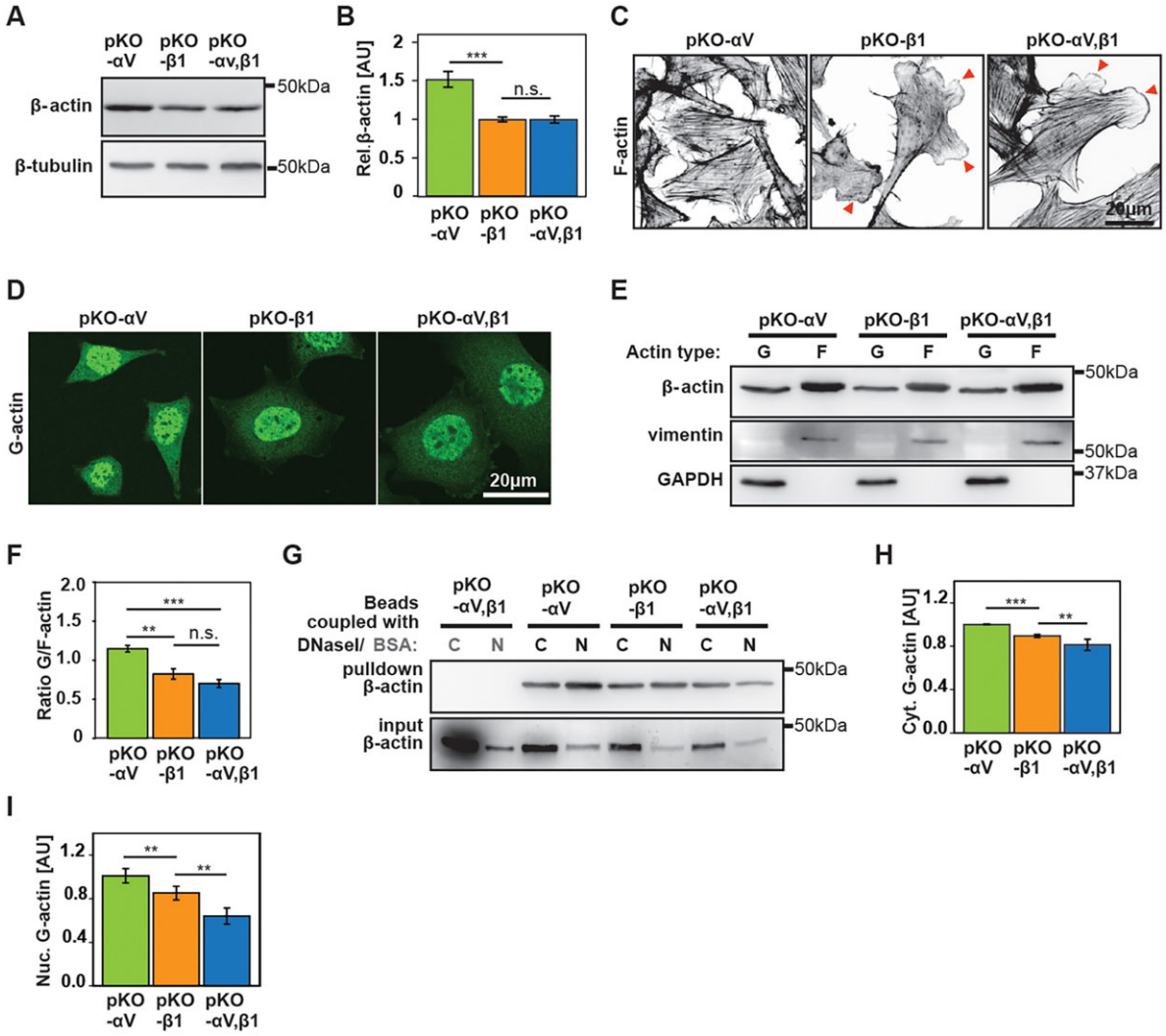

Fig. 1. Fibronectin-bound α5β1- and αV-class integrins control G-actin, F-actin and nuclear MRTF-A levels. (A) Indicated cell lysates were immunoblotted for total actin. β-tubulin was used to control loading. (B) Densitometric quantification of western blots (n=3) is presented as relative total actin levels. (C) Superimposed picture (confocal stack) of indicated cell types immunostained for F-actin (Phalloidin), plated on fibronectin-coated glass surfaces. Arrowheads indicate lamellipodia. (D) Confocal image of indicated cells on fibronectin-coated glass surfaces stained for G-actin with DNaseI–Alexa-Fluor-488. (E) Cell fractionation into soluble (G) and cytoskeletal (F) components followed by western blot analysis with an anti-β-actin antibody. Antibodies against vimentin and GAPDH confirm efficiency of subcellular protein fractionation (representative western blot of nine independent experiments is shown). (F) Ratio of G-actin versus F-actin of the indicated cell types (n=9). (G) G-actin pull downs with DNaseI-coupled Sepharose beads followed by western blot analysis of cytosolic (C) and nuclear (N) components using an anti-β-actin antibody (representative western blot of five independent experiments in technical duplicates is shown). (H,I) Quantification of DNaseI-bound G-actin content in cytoplasmic (H) and nuclear fractions (I) of indicated cell lines (n=5). All error bars represent mean±s.e.m. All P-values were calculated using an unpaired Student's t-test; n.s., not significant; $^{**}P<0.01$; $^{***}P<0.001$.

Journal of Cell Science (2016) 129, 1391-1403 doi:10.1242/jcs.177592

western blot analyses was significantly higher in pKO-αV cells compared with pKO-β1 and pKO-αV,β1 cells (Fig. 1F). To determine monomeric G-actin levels in the cytoplasm and nucleus, we prepared soluble and nuclear cell fractions, respectively, and performed sepharose-coupled DNaseI pull-downs followed by western blotting with anti-β-actin antibodies. The experiments revealed that in both compartments the G-actin levels were highest in pKO-αV, intermediate in pKO-β1 and lowest in pKO-αV,β1 cells (Fig. 1G–I). Importantly, BSA-coupled control beads did not pull down β-actin from either subcellular fraction (Fig. 1G), and FACS analysis excluded nuclear size differences between our cell lines as a possible cause for the different nuclear G-actin contents (Fig. S1B).

Re-analysis of our previously published whole-cell- and phospho-proteome of pKO-αV, pKO-β1 and pKO-αV,β1 cells (Schiller et al., 2013) revealed significantly elevated levels of thymosin β4 (Tβ4) and phospho-serine-3 (pSer3)-cofilin in β1-expressing cells (Fig. S1C–E), indicating that G-actin is sequestered significantly more by the high Tβ4 levels and F-actin severed less by the pronounced inactivation of cofilin in pKO-β1 and pKO-αV,β1 cells compared with pKO-αV cells, which further decreases the free G-actin contents in pKO-β1 and pKO-αV,β1 cells. Taken together, these results show that fibronectin-binding integrin classes differentially regulate cellular G- and F-actin contents.

Fibronectin-binding integrins differentially regulate nuclear MRTF-A levels

MRTF-A is a transcriptional co-activator that is sequestered in the cytoplasm through binding G-actin and released upon actin polymerisation (Posern and Treisman, 2006). Therefore, the different levels of monomeric G-actin in pKO-αV, pKO-β1 and pKO-αV,β1 cells might correlate with different MRTF-A distributions. To test this hypothesis, we stained the cells with specific rabbit polyclonal anti-MRTF-A antibodies (Descot et al., 2009). Indeed, nuclear MRTF-A levels were lowest in pKO-αV, intermediate in pKO-β1 and highest in pKO-αV,β1 cells (Fig. 2A). Treatment with Jasplakinolide, which polymerises free G-actin and stabilises actin filaments (Fig. 2B; Fig. S1F), increased nuclear MRTF-A localisation, whereas treatment with Latrunculin A, which increases monomeric G-actin by depolymerising F-actin, decreased nuclear MRTF-A levels in all three cell lines (Fig. 2C; Fig. S1F). To quantify MRTF-A levels in the cytoplasm and nucleus, the lysates of the respective cell fractions were analysed by immunoblotting using anti-MRTF-A antibodies. Western blot analysis revealed weak nuclear MRTF-A signals in pKO-αV cells, intermediate signals in pKO-β1 cells and highest signals in pKO-αV,β1 cells (Fig. 2D). Similarly, the nuclear/cytoplasmic ratios of MRTF-A were significantly higher in pKO-αV,β1 cells compared with pKO-β1 and especially pKO-αV cells (Fig. 2E). These results show that fibronectin-binding integrin classes differentially regulate nuclear MRTF-A levels.

αV- and β1-class integrins cooperate to control MRTF-A–SRF activity

To test the functional consequences of the different nuclear MRTF-A contents in our three cell lines, we first measured SRF transcriptional activity using luciferase reporter assays (Busche et al., 2008; Sotiropoulos et al., 1999). The assays revealed low SRF reporter activity in pKO-αV cells, 5-fold higher activity in pKO-β1 cells and ∼10-fold higher activities in pKO-αV,β1 cells (Fig. 3A). Serum treatment, which is known to induce nuclear translocation of MRTF-A, increased SRF reporter activities in pKO-β1 and pKO-αV,β1 cells to a much higher extent compared with pKO-αV cells (Fig. S2A), suggesting that β1-integrin-mediated adhesion in cooperation with serum or growth factor-signalling facilitates maximal SRF activity. Overexpression of a dominant-negative version of MRTF-A reduced SRF reporter activity to basal levels in the three cell lines (Fig. S2B), whereas overexpression of a G-actin-binding-deficient MRTF-A (ΔN-MRTF-A) or a constitutive active mDia, which catalyses actin polymerisation, increased MRTF- and/or SRF-driven luciferase activities to similar extents in all three cell lines (Fig. 3A).

Cell spreading defects can also lead to reduced nuclear MRTF-A localisation and SRF reporter activities (Connelly et al., 2010). To exclude that spreading defects of pKO-αV cells (Schiller et al., 2013) were responsible for reduced MRTF-A activities we seeded the three cell lines on fibronectin-coated circular micropatterns with 28 µm or 40 µm diameters (that have twice the surface area of 28 µm sized patterns), and performed SRF luciferase reporter assays and immunostainings. The experiments revealed that pKO-αV cells displayed similarly low SRF reporter activities and nuclear MRTF-A levels on small as well as large fibronectin-coated circular micropatterns, whereas pKO-β1 and pKO-αV,β1 cells exhibited increased SRF activities and nuclear MRTF-A levels on 40-µm-sized micropatterns compared with 28-µm-sized micropatterns (Fig. 3B,C). Taken together these results indicate that reduced spreading of pKO-αV cells is not responsible for their low SRF activity.

Next we investigated whether changes in the activities of fibronectin-binding integrin classes affect SRF reporter activity. First, we activated integrins by treating the cells with Mn^{2+}, which significantly elevated SRF reporter activity in all three cell lines, most prominently in pKO-β1 and pKO-αV,β1 cells (Fig. 3D). Second, we inhibited individual integrin classes in pKO-αV,β1 cells, either with antibodies or peptidomimetics that block specific classes of fibronectin-binding integrins. After seeding pKO-αV,β1 cells on fibronectin (bound by αV- and β1-class integrins), vitronectin (VTN) or gelatin (both ligands bound by αV-class integrins only), they were treated with either anti-α5β1-integrin-blocking antibodies or the αV-class-specific small molecule inhibitor cilengitide and immunostained for MRTF-A. The experiments showed that inhibition of either α5β1 or αVβ3 integrins on fibronectin-adherent pKO-αV,β1 cells significantly reduced nuclear MRTF-A levels and thus phenocopied the situation in pKO-αV or pKO-β1 cells (Fig. 3E; Fig. S2C), and confirmed the synergistic role of both fibronectin-binding integrin classes for nuclear MRTF-A accumulation. Similarly, when pKO-αV,β1 cells were seeded on VTN and gelatin, they showed weak nuclear MRTF-A signals, which were not further decreased by blocking the function of α5β1 integrin (Fig. S2C). Treatment of VTN- or gelatin-seeded pKO-αV, β1 cells with cilengitide blocked cell adhesion (Fig. S2C). Taken together these data indicate that αV- and β1-class integrins cooperate to maximise nuclear accumulation of MRTF-A and SRF activity.

αV- and β1-class integrins cooperate to promote transcription of MRTF–SRF target genes

The high nuclear MRTF-A content and SRF activity in pKO-αV,β1 cells suggest that MRTF-A–SRF-induced gene transcription is controlled, at least in part, by a cooperation of αV- and β1-class integrins. To test this possibility, we compared published MRTF and SRF transcriptomes (Balza and Misra, 2006; Cooper et al., 2007; Descot et al., 2009; Philippar et al., 2004; Selvaraj and Prywes, 2004; Sun et al., 2006; Zhang et al., 2005) with the whole cell proteome data of pKO-αV, pKO-β1 and pKO-αV,β1 cells (Schiller et al., 2013) and found a large number of MRTF–SRF

Journal of Cell Science (2016) 129, 1391-1403 doi:10.1242/jcs.177592

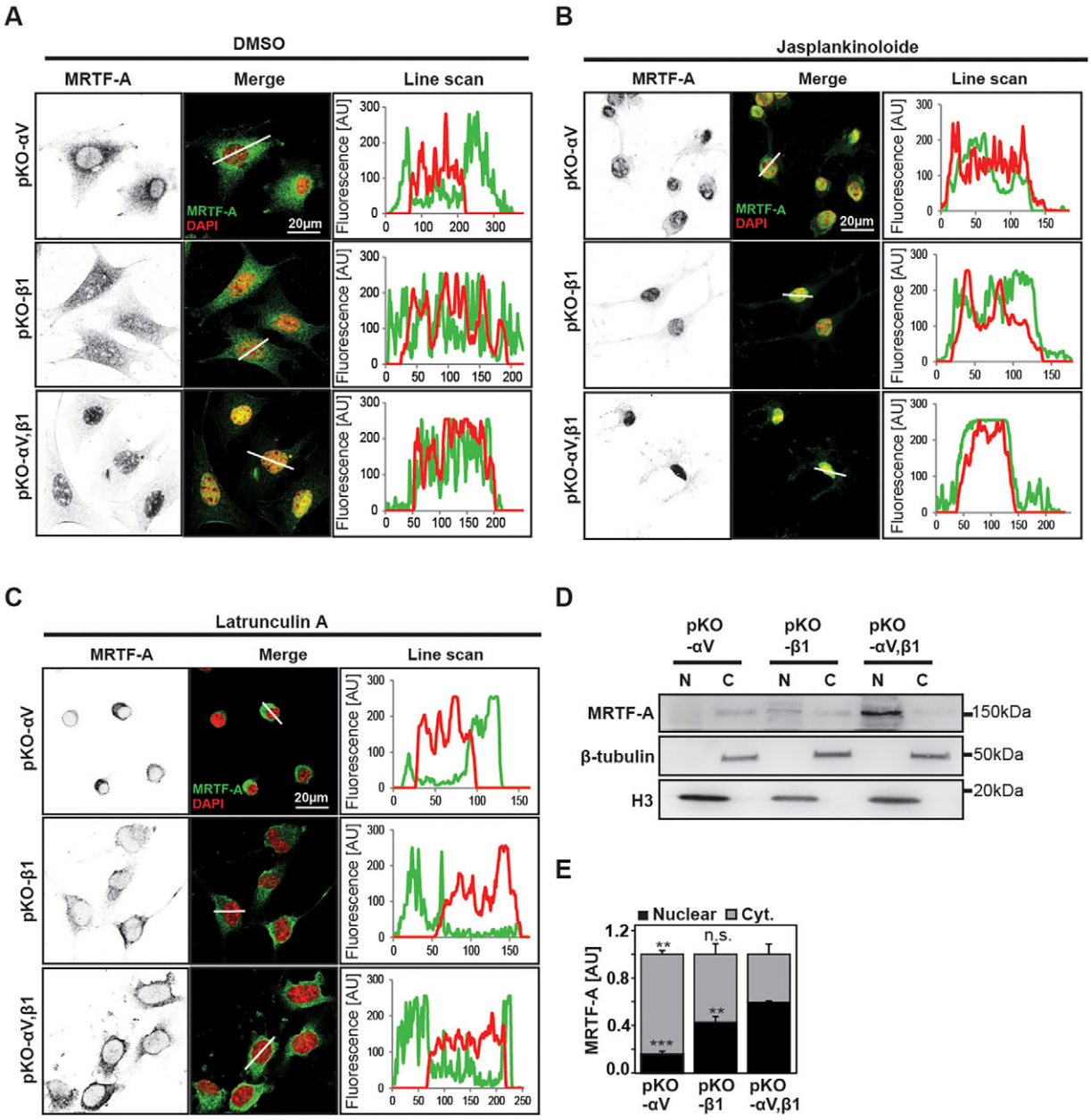

Fig. 2. Fibronectin-binding integrins differentially regulate nuclear MRTF-A levels. (A–C) MRTF-A immunostaining of indicated cell lines plated on fibronectin-coated glass coverslips. The cell lines were either left untreated (A) or were treated with 100 nM Jasplakinolide (B) or 500 nM Latrunculin A (C). The merged images demonstrate an overlay of MRTF-A and nuclear (DAPI) signal. Line scan analysis was used for co-localisation analysis of nuclear DAPI (red) and MRTF-A (green) signals. (D) Cell fractionation into nuclear (N) and cytosolic (C) components followed by western blot analysis with an anti-MRTF-A antibody. Antibodies against β-tubulin and Histone-H3 confirm efficiency of subcellular protein fractionation (representative western blot of nine independent experiments is shown). (E) Quantification of MRTF-A content in nuclear and cytosolic (Cyt.) cell fractions of indicated cell lines (*n*=9). All error bars represent mean±s.e.m. All *P*-values were calculated using an unpaired Student's *t*-test; n.s., not significant; ***P*<0.01; ****P*<0.001.

targets, including SRF itself, and focal adhesion proteins such as vinculin and talin-1, enriched in pKO-β1 and pKO-αV,β1 cells (Table 1). The increased levels of SRF, talin-1 and vinculin mRNA and protein in pKO-β1 and pKO-αV,β1 cells were confirmed by qRT-PCR and western blotting (Fig. 4A,B).

We also noted that the ISG15 mRNA and protein was significantly higher in pKO-αV,β1 cells, compared with pKO-αV cells (Fig. 4A, Table 1) and that its mRNA was previously shown to be downregulated upon SRF deletion in mouse embryonic stem cells (ESCs) (Philippar et al., 2004). Western blotting confirmed high ISG15 levels in pKO-αV,β1, intermediate levels in pKO-β1 and low levels in pKO-αV cells (Fig. 4B,C). Although it has been reported that ISG15 can be secreted we did not detect ISG15 in the supernatant of either cell line (Fig. S3A). Immunostainings also detected high ISG15 levels in pKO-αV,β1 and low levels in pKO-αV cells. The immunostaining also demonstrated that ISG15 colocalised with F-actin fibres, with the actin cortex in membrane protrusions (Fig. 4D) and with paxillin in focal adhesions of unroofed cells (Fig. 4E). ISG15 is an ubiquitin-like modifier, whose expression is induced by type I (α and β) interferons (Farrell et al., 1979; Haas et al., 1987). Whereas ELISA and qRT-PCR excluded expression of interferon α and β by pKO-αV,β1 cells as cause for the

Journal of Cell Science (2016) 129, 1391-1403 doi:10.1242/jcs.177592

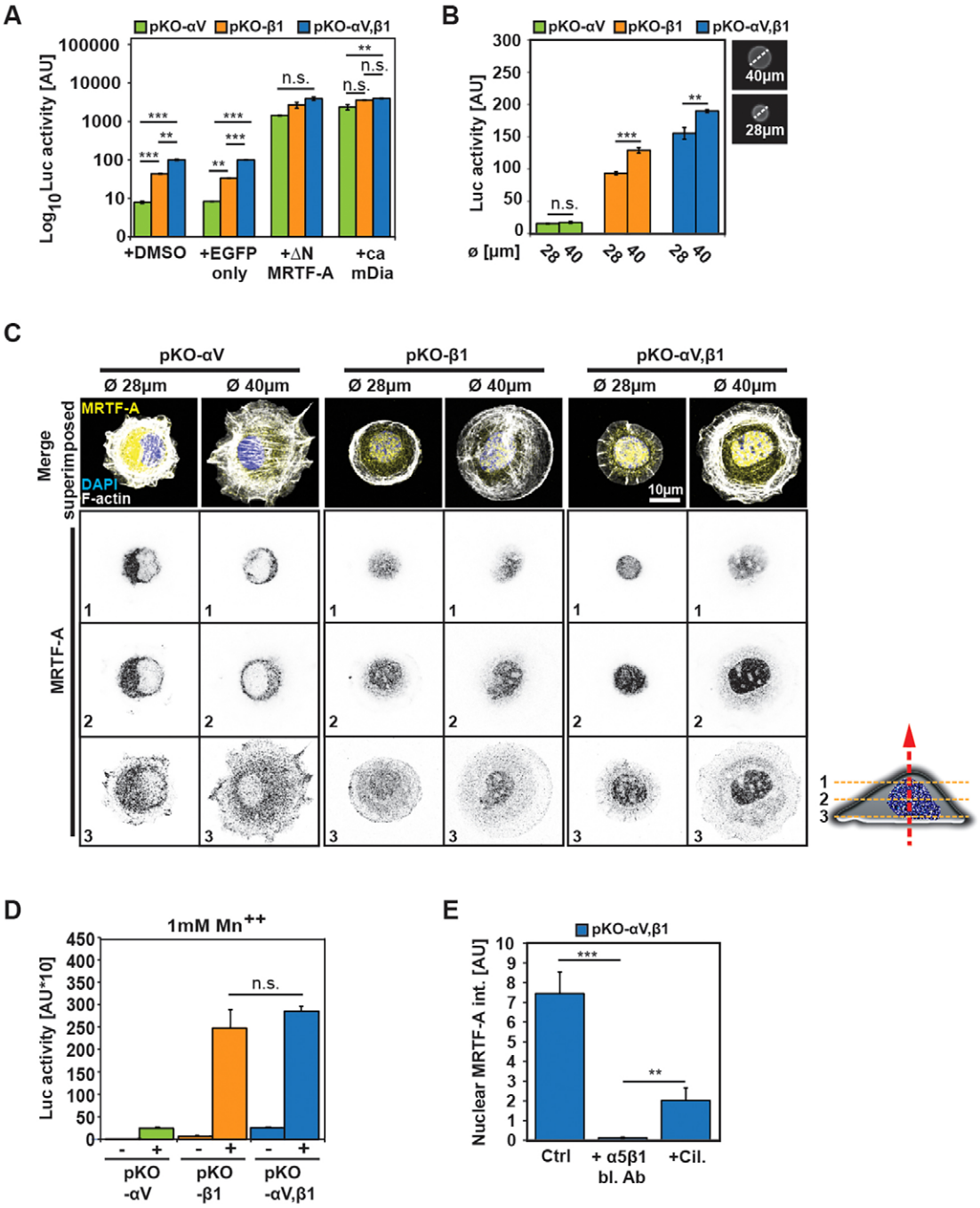

Fig. 3. αV-class integrins cooperate with α5β1 integrin to induce MRTF-A/SRF activity. (A) SRF-driven luciferase reporter activity in cells plated on fibronectin and treated with DMSO, transfected with EGFP, constitutive active (ca)-MRTF-A (ΔN-MRTF-A) or ca-mDia constructs (n=4). (B) SRF-driven luciferase reporter activity in cells plated on circular fibronectin-coated micropatterns with either 40 µm or 28 µm diameter (n=3 independent experiments). (C) Z-stacks of immunostained cells seeded on circular fibronectin-coated micropatterns with indicated diameters. The cartoon on the right illustrates the position of the indicated stack. The merged picture displays an overlay of MRTF-A (yellow), F-actin (white) and nuclear staining (DAPI, blue). (D) SRF-driven luciferase reporter activity in indicated cells treated with Mn^{2+} (n=5). (E) Quantification of nuclear MRTF-A signal intensities in fibronectin-plated pKO-αV,β1 cells untreated or treated with α5β1-integrin-blocking antibody and cilengitide. All error bars represent mean±s.e.m. All P-values were calculated using an unpaired Student's t-test; n.s., not significant; **P<0.01; ***P<0.001.

high ISG15 levels (Fig. S3B–E), Poly(I:C) treatment induced interferon α and β expression (Fig. S3B–E), which in turn triggered a strong *Isg15* expression (Fig. S3F).

To demonstrate that *Isg15* is an MRTF–SRF target gene, we searched for SRF consensus binding sites (CArG box) in the mouse *Isg15* locus and performed chromatin immunoprecipitation (ChIP) assays. The mouse *Isg15* gene contains a CArG box in the first intron (Fig. 4F). The MRTF–SRF targets *vinculin* (*Vcl*) and *talin-1* (*Tln1*) were used as controls and *gapdh* as a negative control (Vartiainen et al., 2007). ChIP samples were obtained using either anti-MRTF-A, anti-SRF or control IgG antibodies and the resulting chromatin DNA samples were PCR amplified with primers flanking the indicated CArG boxes of *Isg15*, *Tln1* and *Vcl* (Fig. 4F). As expected, the *gapdh* gene was not amplified

Journal of Cell Science (2016) 129, 1391-1403 doi:10.1242/jcs.177592

Table 1. Qualitative comparison of MRTF/SRF target genes to the proteome data of pKO-αV, pKO-β1 and pKO-αV,β1 cells (published in Schiller et al., 2013)

SRF target genes			Proteome enriched		
Gene name	Annotation	Source	pKO-αV	pKO-β1	pKO-αV,β1
ACTA1	Skeletal alpha actin	1,2,6	n.f.	n.f.	n.f.
ACTA2	Smooth muscle alpha actin	1,2,6	n.f.	n.f.	n.f.
ACTC	Alpha-cardiac actin	2	n.f.	n.f.	n.f.
ACTC1	Actin, alpha cardiac muscle 1	1,5,6	n.f.	n.f.	n.f.
ACTG	Actin, cytoplasmic 2	2	n.f.	n.f.	n.f.
ACTN1	Alpha-actinin-1	4	–	+	+
CAPZA3	F-actin-capping protein subunit alpha-3	4	n.f.	n.f.	n.f.
CFL1	Cofilin, non-muscle isoform	4	–	+	+
CFL2	Cofilin2, muscle	1,4	n.f.	n.f.	n.f.
DSTN	Destrin, Actin-depolymerizing factor, ADF	4,6,7	–	+	+
ENAH, MENA	Protein enabled homolog	1	n.f.	n.f.	n.f.
EPLIN	LIM domain and actin-binding protein 1	6	–	+	+
FBLN5	Fibulin-5	4	n.f.	n.f.	n.f.
FHL1	Four and a half LIM domains protein 1	4,6	n.f.	n.f.	n.f.
FHL2	Four and a half LIM domains protein 2	2,4	–	+	+
FLNA	Filamin A	4	–	+	+
FLNC	Filamin C	4	n.f.	n.f.	n.f.
FNBP1	Formin-binding protein 1	1	–	+	+
IQGAP	Ras GTPase-activating-like protein IQGAP1		–	+	+
ISG15	Interferon-induced 15 kDa protein	2	–	+	+
ITGA1	Integrin alpha 1	7	n.f.	n.f.	n.f.
ITGA5	Integrin alpha5	4,6	–	+	+
ITGA9	Integrin alpha 9	1,5	n.f.	n.f.	n.f.
ITGB1	Integrin beta 1	1	–	+	+
ITGB1BP2	Integrin beta 1 binding protein 2 (melusin)	1,4,7	n.f.	n.f.	n.f.
LPP	LIM domain-containing preferred translocation partner in lipoma	2,6	–	+	+
MAP3K14	Mitogen-activated protein kinase kinase kinase 14	5,6	n.f.	n.f.	n.f.
MAP3K4	Mitogen-activated protein kinase kinase kinase 4	5	n.f.	n.f.	n.f.
MAPK10	Mitogen-activated protein kinase 10, JNK3	5	n.f.	n.f.	n.f.
MYH11	Myosin heavy chain, smooth muscle isoform, SMMHC	7	n.f.	n.f.	n.f.
MYH6	Myosin heavy chain, cardiac muscle alpha isoform, MyHC-alpha	1	n.f.	n.f.	n.f.
MYH7	Myosin heavy chain, cardiac muscle beta isoform, MyHC-beta	1	n.f.	n.f.	n.f.
MYH9	Non-muscle myosin heavy chain A, NMMHC-A, NMMHC-lia	6,7	–	+	+
MYL3	Myosin light chain 1, slow-twitch muscle B/ventricular isoform, MLC1SB	1,5	n.f.	n.f.	n.f.
MYL4	Myosin light chain 1, atrial/fetal isoform, MLC1A	1	n.f.	n.f.	n.f.
MYL9	Myosin light chain 9, smooth muscle	1,5	+	–	+
PDLIM5	Enigma homolog, Enh	4	–	+	+
PDLIM7	Enigma	1,6	–	–	+
PFN1	Profilin-1	4	n.f.	n.f.	n.f.
SRF	Serum response factor	1,3	–	+	+
SVIL	Supervillin	1,7	–	+	+
TLN	Talin	4	–	+	+
TRIP6	Zyxin-related protein 1	4	–	+	+
VCL	Vinculin	2,3,6,7	–	+	+
VIL1	Villin-1	6	n.f.	n.f.	n.f.
ZYX	Zyxin	3	+	–	+

Data mining and comparison of seven different MRTF–SRF target gene screening approaches were manually filtered for association with focal adhesion and actin functions and co-localisation. A qualitative comparison with the pKO-cell proteome was performed. +, enriched; –, not enriched, n.f., not found. Data sources cited: (1) Balza and Misra, 2006; (2) Philippar et al., 2004; (3) Selvaraj and Prywes, 2004; (4) Sun et al., 2006; (5) Zhang et al., 2005; (6) Descot et al., 2009; and (7) Cooper et al., 2007.

and control rabbit IgG precipitates did not produce PCR products (Fig. 4G,H).

αV- and β1-class-integrin-induced MRTF-A–SRF activity and ISG15 levels promote cell migration

MRTF-A–SRF and ISG15 are upregulated in cancer and promote tumour cell invasion (Desai et al., 2012; Kressner et al., 2013). To test whether the invasive properties of MRTF-A and ISG15 are associated with and triggered by β1-integrin-mediated adhesion we compared the integrin expression profile, nuclear MRTF-A and ISG15 levels between the non-invasive MCF-7 (luminal type) and the low invasive MDA-MB-468 (basal-A type) and highly invasive MDA-MB-231 (basal-B type) breast carcinoma cell lines (Neve et al., 2006). FACS analysis revealed significantly higher α5 and β1 integrin levels and higher β1 integrin activity (shown with the activation-epitope binding 9EG7 antibody) on MDA-MB-231 cells compared with MCF-7 cells (Fig. 5A). Interestingly, the low invasive MDA-MB-468 cells demonstrated no detectable α5 integrin and low total and active β1 integrin surface levels (Fig. 5A). The levels of αV integrin were significantly elevated in MDA-MB-468 and MCF-7 cells compared with MDA-MB-231 cells (Fig. 5A). To test whether the high β1 integrin levels and activity in MDA-MB-231 cells are associated with high nuclear MRTF-A activity we stained for F-actin and MRTF-A, and

Journal of Cell Science (2016) 129, 1391-1403 doi:10.1242/jcs.177592

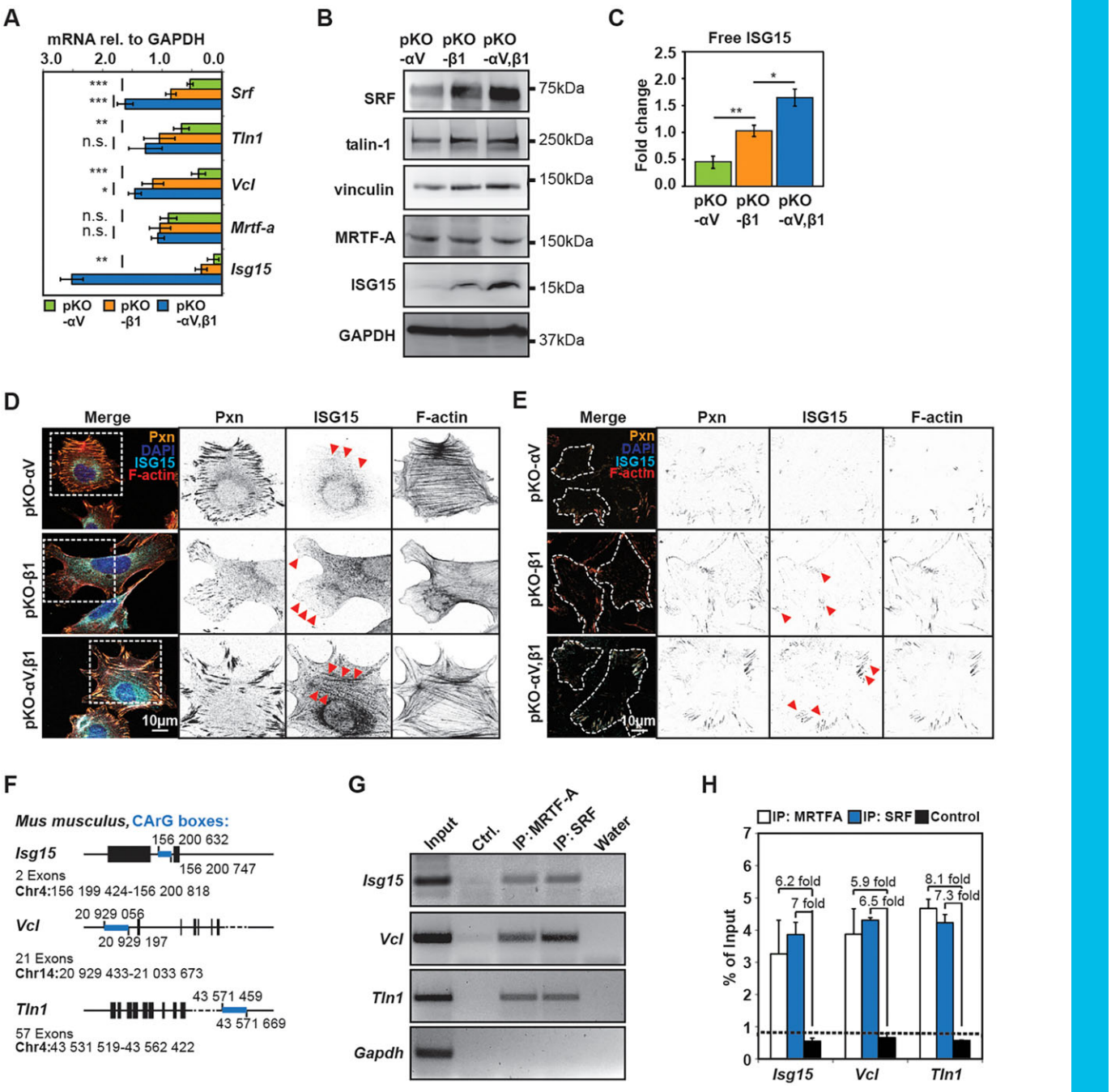

Fig. 4. αV- and β1-class integrins induce expression of MRTF-A–SRF target genes. (A) Quantitative real-time PCR of *Srf*, *Tln1*, *Vcl, Mrtf-a* and *Isg15*. mRNA levels are shown relative to *gapdh* levels (n>3; independent RNA isolations). (B) Western blot analysis of SRF, talin-1, vinculin, MRTF-A and ISG15. GAPDH was used as a loading control. (C) Densitometric analysis of free ISG15 protein in indicated cell lines (n=5). (D) Immunostaining of indicated cell lines for paxillin (Pxn), ISG15, F-actin and DAPI. Arrowheads indicate co-localisation of F-actin and ISG15 signals. (E) Immunostaining of ISG15, paxillin, F-actin and nucleus (DAPI) in focal adhesions of cross-linked and unroofed cells. The merged images display an overlay of ISG15, paxillin, F-actin and DAPI. (F) Scheme indicating the location of CArG boxes (blue) in *Isg15*, *Vcl* and *Tln1* gene loci, exons are shown as black boxes. (G,H) Chromatin immunoprecipitations with anti-MRTF-A, -SRF or rabbit IgG control antibodies. The CArG box of *Isg15*, *Vcl*, *Tln1* (and *gapdh* locus as a control) were amplified by conventional PCR and separated by agarose gel electrophoresis. (H) Real-time PCR was performed from three independent chromatin preparations and IPs. Shown is the relative quantitation of *Isg15*, *Vcl* and *Tln1* signal relative to input chromatin. All error bars represent mean±s.e.m. All *P*-values were calculated using an unpaired Student's *t*-test; **P*<0.05; ***P*<0.01; ****P*<0.001.

investigated SRF activity with luciferase reporter assays. We found that MDA-MB-468 cells spread poorly, contained cortical F-actin rings and showed high cytoplasmic and low nuclear MRTF-A signals, whereas MCF7 cells were well spread, formed tight, F-actin-rich cell–cell contacts and contained MRTF-A in the cytoplasm as well as in the nucleus (Fig. 5B). By contrast, MDA-MB-231 cells were not adhering to each other, contained numerous F-actin stress fibres throughout the cytoplasm and almost the entire pool of MRTF-A protein was detected in the nucleus (Fig. 5B,C). In line with high nuclear MRTF-A levels, MDA-MB-231 cells also displayed significantly higher SRF reporter activity (Fig. 5D) and expressed significantly higher levels of MRTF–SRF target gene transcripts

Journal of Cell Science (2016) 129, 1391-1403 doi:10.1242/jcs.177592

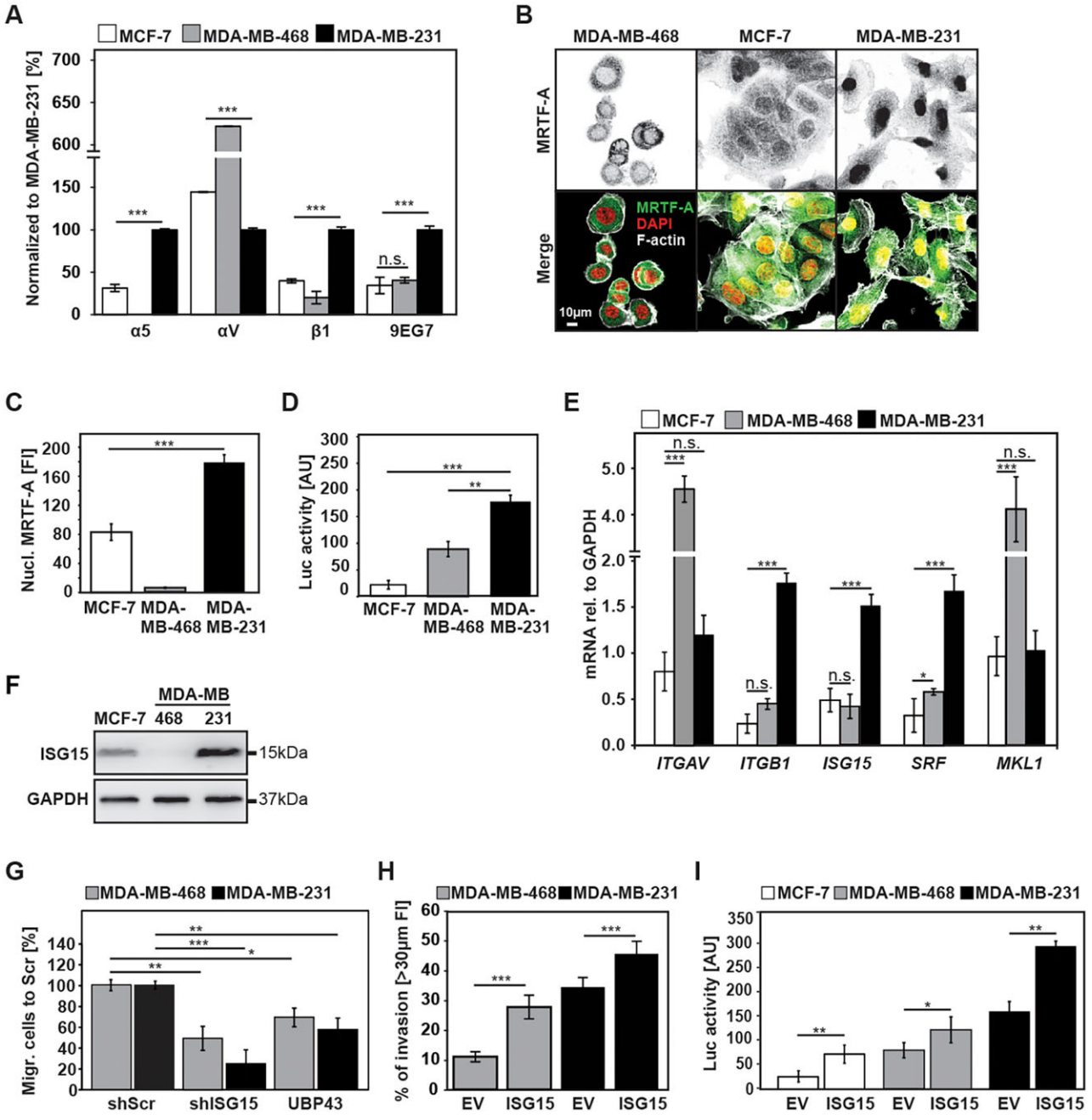

Fig. 5. αV- and β1-class-integrin-induced MRTF-A–SRF activity and ISG15 levels promote breast cancer cell migration. (A) FACS analysis of α5, αV and β1 integrin surface levels and active β1 integrin (using the 9EG7 antibody) in MCF-7, MDA-MB-468 and MDA-MB-231 cells. (B) Immunostaining of MRTF-A in MCF-7, MDA-MB-231 and MDA-MB-468 breast carcinoma cells seeded on fibronectin-coated glass coverslips. The merged images display an overlay of MRTF-A, F-actin and nuclear staining (DAPI). (C) Intensity of nuclear MRTF-A signal (n=2 independent experiments; >129 immunostained cells per cell line were analysed). (D) SRF-driven luciferase reporter assay of MCF-7, MDA-MB-468 and MDA-MB-231 cells (n=3). (E) qRT-PCR for *ITGAV*, *ITGB1*, *ISG15*, *SRF*, and *MKL1* in indicated breast cancer cell lines. Shown is the quantitation relative to *gapdh* (n=3, 3 independent mRNA isolations). (F) Western blot of MCF-7, MDA-MB-231 and MDA-MB-468 cells with anti-ISG15-specific antibody. GAPDH was used as a loading control. (G) Quantification of fibronectin-coated trans-well migration assay with MDA-MB-231 and MDA-MB-468 cells expressing scrambled shRNA (shScr), *ISG15*-specific shRNAs, or the ISG15-specific UBP43 peptidase (n=4). The data is expressed as a percentage of trans-well-migrated cells compared with shScr control. (H) Quantification of Matrigel invasion by MDA-MB-468 and MDA-MB-231 cells transduced with either empty vector (EV) or an ISG15 expression construct. Invasive migration was quantified by measuring the fluorescence intensity of cells invading the Matrigel plug deeper than 30 μm. The invasion capacity was expressed as percentage of total fluorescence intensity of all cells within the plug. At least three independent experiments were performed. (I) SRF luciferase reporter assay of MCF-7, MDA-MB-468 and MDA-MB-231 cells transfected with empty vector or ISG15 expression construct (n=3). All error bars represent mean±s.e.m. All P-values were calculated using an unpaired Student's t-test; n.s., not significant; *P<0.05; **P<0.01; ***P<0.001.

(Fig. 5E). The free levels of ISG15 protein were highest in MDA-MB-231, lowest in MDA-MB-468 and intermediate in MCF7 cells (Fig. 5F). Interestingly, the ISGylation of target proteins was highest in MDA-MB-231, intermediate in MDA-MB-468 and lowest in MCF-7 cells (Fig. S4A) indicating that MDA-MB-468 cells use their entire low ISG15 pool to ISGylate proteins.

Journal of Cell Science (2016) 129, 1391-1403 doi:10.1242/jcs.177592

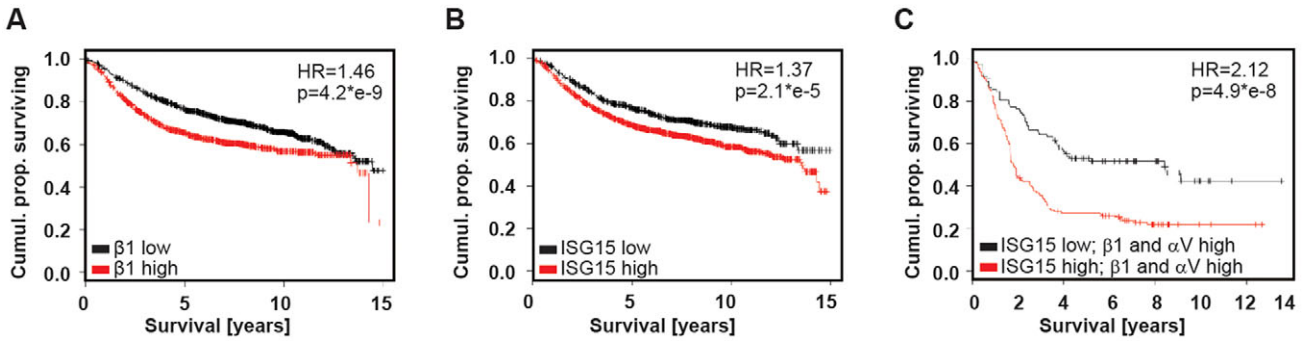

Fig. 6. High integrin and ISG15 expression correlates with poor prognosis of breast cancer patients. (A,B) Kaplan–Meier analysis indicates a decreased disease-free survival of breast cancer patients with high *integrin β1* (A) or high *ISG15* (B) levels. (C) The disease-free survival is further decreased for individuals expressing high levels of ISG15 and high levels of α5 and β1 integrins.

The invasive properties of MDA-MB-231 cells have been shown to depend on the expression of MRTF-A (Hu et al., 2011; Medjkane et al., 2009). To test whether ISG15 is required for SRF–MRTF-A-induced cell invasion, we depleted ISG15 or overexpressed the de-ISGylase UBP43 in MCF-7, MDA-MB-468 and MDA-MB-231 cells and performed trans-well migration assays through fibronectin-coated membranes and 3D-Matrigel invasion assays. MCF-7 cells were unable to invade through fibronectin-coated membranes and invade 3D-Matrigels (not shown). MDA-MB-231 and -468 cells, however, efficiently migrated through fibronectin-coated membranes, which significantly diminished upon shRNA-mediated depletion of ISG15 or overexpression of the de-ISGylase UBP43 (Fig. 5G; Fig. S4B). Furthermore, MDA-MB-231 cells, and to a lesser extent MDA-MB-468 cells, invaded 3D-Matrigels, which was further enhanced upon overexpression of ISG15 (Fig. 5H; Fig. S4C). Interestingly, overexpression of ISG15 significantly increased basal SRF activities in MCF-7, MDA-MB-468 and MDA-MB-231 cells (Fig. 5I), pointing to a positive feed-forward loop between integrin-mediated adhesion signalling, MRTF−SRF and ISG15. In line with a potential feed-forward loop, the decreased migration of MRTF-A-depleted MDA-MB-231 cells through fibronectin-coated membranes could not be improved by simultaneously overexpressing ISG15 (Fig. S4D).

Our results suggest that high levels of *β1 integrin* and *ISG15* represent prognostic markers for breast cancer patients. To evaluate this possibility, we consulted microarray databases of breast cancer samples and correlated *αV integrin*, *β1 integrin* and *ISG15* transcript levels with patient survival. The analyses clearly revealed that individuals with high expression of *β1 integrin* or *ISG15* displayed a significant increase in the hazardous ratio (HR) compared with individuals with low levels of either transcript (Fig. 6A,B). Importantly, however, individuals with high levels of *αVβ1 integrin* and *ISG15* transcripts in their tumour samples showed a pronounced reduction in disease-free survival rate compared with individuals with low *ISG15* levels (Fig. 6C). These findings demonstrate that integrin-mediated MRTF-A–SRF–ISG15 signalling is elevated in breast cancer and associated with a poor prognosis.

DISCUSSION

Metastasis is initiated with the detachment of individual cancer cells from the tumour cell aggregate followed by invasion into the surrounding tissue, entry into the circulation and finally settlement in a distant organ. The process of tumour cell invasion is crucially dependent on the selection of tumour cells that are able to survive without tumour stroma, on the release of proteases that degrade and remodel the tumour- and tissue-derived extracellular matrix (ECM), and on cell adhesion molecules such as integrins (Hood and Cheresh, 2002). Integrins constitute the core components of the invasive machinery of cancer cells. They regulate the activity of small GTPases, actin binding, bundling and modifying proteins to enable cytoskeletal dynamics, membrane protrusions and invadopodia formation (Bishop and Hall, 2000; Hall, 2012; Hoshino et al., 2013; Murphy and Courtneidge, 2011). Interestingly, a recent paper showed that integrins also regulate the nuclear translocation of MRTF-A and induce MRTF-A–SRF target gene expression (Plessner et al., 2015). Because tumour cells express different types of integrins, it is unclear whether and how they co-operate to achieve maximal efficiency in tissue invasion and migration. The aim of the present study was to define integrin subfamilies and the signalling pathways involved in tumour cell invasion.

We have recently engineered a fibroblast-like cell line that allows expression of the fibronectin-binding integrins αVβ3 and/or α5β1. These cell lines were used to demonstrate that αVβ3 and α5β1 integrins control actomyosin-based cell contractility in a cooperative manner (Schiller et al., 2013). In the present study we also observed that the cells expressing αVβ3 and α5β1 integrins (pKO-αV,β1 cells) most markedly decrease their G-actin pool, which results in the nuclear translocation of the G-actin-binding transcriptional transactivator MRTF-A. The nuclear accumulation of MRTF-A allows binding to the transcription factor SRF and transcriptional activation of MRTF-A–SRF target genes, which comprise known target genes such as actin, vinculin and filamins (Esnault et al., 2014), as well as newly discovered targets such as talin-1 and ISG15, which contain functional CArG boxes known to bind the MRTF-A–SRF complex (Olson and Nordheim, 2010).

Our findings show that ISG15 is particularly highly elevated when αVβ3 and α5β1 integrins are co-expressed and bind fibronectin. ISG15 is a ubiquitin like modifier protein that is conjugated to specific lysine residues of target proteins (Kerscher et al., 2006). *ISG15* expression, which is elevated in almost all tumours investigated so far (www.oncomine.org), is thought to be induced by type I interferons (Farrell et al., 1979; Haas et al., 1987). Because the tumour stroma is infiltrated by immune cells, it is believed that they are the source of interferon α and β production and hence the trigger for the high ISG15 expression in cancer cells (van der Veen and Ploegh, 2012). Although immune-cell-derived interferon α and/or β strongly promotes expression of ISG15 in tumours, it remained unknown why high ISG15 levels persisted in tumour cells isolated and cultured *ex vivo* in the absence of immune cells and interferons (Han et al., 2002; Hermeking et al., 1997; Lock

Journal of Cell Science (2016) 129, 1391-1403 doi:10.1242/jcs.177592

et al., 2002). Based on our findings we propose that synergistic αVβ3- and α5β1-integrin-induced nuclear translocation of MRTF-A and activation of SRF are responsible for the high *ISG15* transcription *ex vivo*.

ISG15 is conjugated to proteins (ISGylation) in a multistep process that requires E1, E2 and E3 enzymes and is comparable to the protein-ubiquitylation pathway (Haas et al., 1987; Lenschow et al., 2005; Loeb and Haas, 1992; Morales and Lenschow, 2013; Okumura et al., 2008; Yuan and Krug, 2001). Protein modifications with ISG15 are reversible and can be removed (or de-ISGylated) by the ISG15 de-conjugating peptidase Ubp43 (Malakhov et al., 2002). Protein ISGylation can alter protein function; for example, ISGylation of filamin-B can release filamin-B-bound Rac1, MKK4 and MEKK1, leading to the termination of JNK signalling and inhibition of apoptosis (Jeon et al., 2009). By contrast, it has also been shown that ISG15 modification can stabilise proteins by inhibiting ubiquitin-specific E2 enzymes (Desai et al., 2006; Malakhova and Zhang, 2008; Okumura et al., 2008) or by competing with ubiquitin for lysine residues on common target proteins (Liu et al., 2003). Finally, ISGylation has been shown to inhibit protein translation by either increasing the cap-structure-binding activity of the ISGylated translational suppressor 4EHP (Okumura et al., 2007) or by downregulating eIF2α through ISGylation of dsRNA-dependent protein kinase (PKR) (Okumura et al., 2013).

The high expression of ISG15 in tumour cells *in vivo* and *ex vivo* indicates that ISGylation-dependent inhibition of apoptosis or stabilisation of certain oncogenic proteins represents a tumour-promoting function in primary tumours where interferon α and β levels are high, as well as during metastasis when interferon levels decrease. Hence, it is conceivable that during invasion and metastasis for example, cooperative signalling via αVβ3 and α5β1 integrins compensates for low interferon levels to sustain high ISG15 expression. Previously published mass spectrometry analyses of ISG15-modified proteins (ISGylome) in tumour cells revealed that actin, actin regulatory and focal adhesion proteins (filamin-B, vinculin, talin-1) can be ISGylated (Durfee et al., 2010). It is therefore possible that αVβ3- and α5β1-integrin-mediated signalling has two major consequences for tumour cell invasion; αVβ3 and α5β1 integrins activate GTPases leading to polymerisation of F-actin networks and stress fibres, which are essential for membrane protrusions, cell contractility and adhesion reinforcement. In addition, the consumption of G-actin for the formation of different F-actin networks results in liberation and nuclear translocation of MRTF-A, binding to SRF and transcription of cytoskeletal, focal adhesion proteins and ISG15 itself. ISG15 modifies various proteins, including focal adhesion proteins and actin-binding or -modifying proteins to increase their stability and/or improve their function (Fig. 7). Such a feed-forward circuit operates in mouse fibroblasts as well as in invading MDA-MB-231 breast cancer cells. The metastatic breast cancer cell line MDA-MB-231 expressed significantly more α5β1 integrin, contained higher levels of nuclear MRTF-A, showed an elevation of ISG15-conjugated proteins in whole-cell lysates and performed better in fibronectin-based trans-well migration assays and in 3D-Matrigel invasion assays than the less invasive MDA-MB-468 or non-metastatic MCF7 cells. We could also demonstrate that the ability of the invasive MDA-MB-231 and MDA-MB-468 cells to migrate relies on ISG15 expression and ISGylation and that ISG15 overexpression enhances 3D-Matrigel invasion of both, MDA-MB-231 and MDA-MB-468 cancer cells. Most importantly, transcriptome analyses of breast cancer samples from large cohorts of patients revealed a statistically highly significant association between disease free patient survival and high *β1 integrin*, *αV-integrin* and *ISG15* transcript levels. These findings suggest that breast cancer cells with high integrin levels are selected in a primary tumour mass, which renders them independent of decreasing interferon and growth factor signals for sustaining nuclear MRTF-A activity, ISG15 expression and metastatic potential.

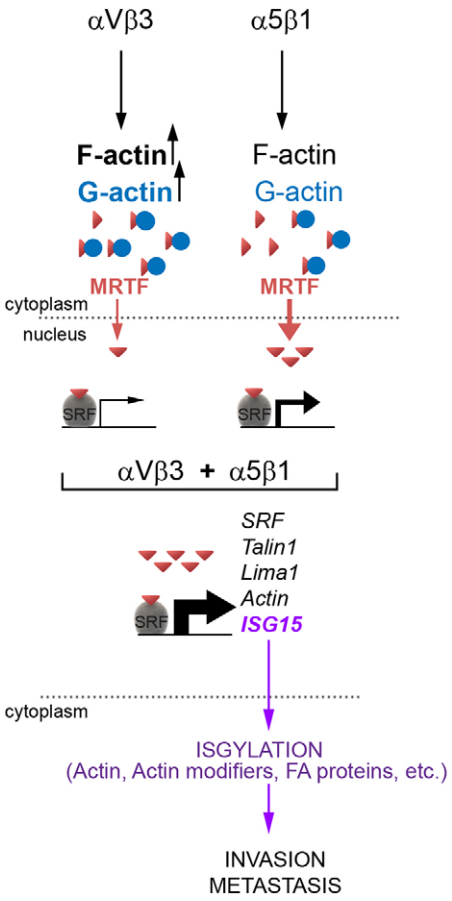

Fig. 7. Schematic of α5β1- and αV-class integrin expression pathways leading to increased invasion and metastasis. α5β1- and αV-class integrins synergistically induce MRTF/SRF activity, downstream gene expression, amongst others ISG15, leading to protein ISGylation and enhanced cancer migration and invasion.

MATERIALS AND METHODS

Cell lines

The generation of pKO-αV, pKO-β1 and pKO-αV,β1 cell lines was reported previously (Schiller et al., 2013). The breast cancer cell lines MDA-MB-231 and MCF-7 were purchased from ATCC (http://www.lgcstandards-atcc.org/Products/Cells_and_Microorganisms/Cell_Lines.aspx), MDA-MB-468 cells were obtained from Dr Axel Ullrich (MPI Biochemistry, Martinsried).

Immunostainings and surface coating

For immunofluorescence microscopy, cells were seeded on ECM-coated micropatterns or glass surfaces (coating: 5 µg/ml fibronectin (Calbiochem) or 1% gelatin (Sigma) or 10 µg/ml vitronectin (STEMCELL Technologies) in PBS) in DMEM (GIBCO by Life Technologies) containing 10% FCS at 37°C, 5% CO_2. To culture cells on micropatterns the culture medium contained 0.5% FCS. After indicated time points the medium was soaked off, and cells were fixed with 3% PFA in PBS for 10 min at room temperature, washed with PBS, blocked with 1% BSA in PBS for 1 h at room temperature and then incubated with antibodies in a solution of 0.1% Triton X-100, 3% BSA in PBS. The fluorescent images were collected with

Journal of Cell Science (2016) 129, 1391-1403 doi:10.1242/jcs.177592

a laser scanning confocal microscope (Leica SP5). For visualization of G- and F-actin structures, we followed a previously published protocol (Small et al., 1999).

Antibodies

All antibodies are listed in Table S2.

Crosslinking

Enrichment for focal-adhesion-associated proteins was achieved by briefly fixing the ventral cell cortex using DSP crosslinker [DTSP; dithiobis (succinimidyl propionate)], followed by removal of non-crosslinked proteins and big organelles by stringent cell lysis and hydrodynamic sheer flow washing.

Cell fractionation

For cell fractionation the ProteoExtract® Cytoskeleton Enrichment and Isolation Kit (Millipore), and for G-actin and F-actin analyses the In Vivo Assay Biochem Kit (Cytoskeleton, Inc.) were used. For the centrifugation-based method to isolate the nuclei, cells were washed with PBS and harvested in a buffer containing 250 mM sucrose, 10 mM HEPES and 1.5 mM EDTA. With the help of a syringe and a 26 Ga needle (Terumo) cells were disrupted further. After centrifugation the pellet (nuclei fraction) was washed five times with a buffer containing 20 mM Tris, 0.1 mM EDTA and 2 mM $MgCl_2$. The pellet was resuspended in FACS buffer or staining solution for immunostaining.

G-actin pulldown by DNaseI

DNaseI (Sigma-Aldrich) was covalently linked to CNBr-activated Sepharose beads (Sigma-Aldrich) at a concentration of 1 mg/ml according to the manufacturer's protocol. BSA–sepharose beads, which served as control, were prepared in the same way. For G-actin pulldown, nuclear and cytosolic fractions were incubated with 35 µl of DNaseI- or BSA-coupled Sepharose beads in a volume of 200 µl overnight at 4°C in an end-over-end mixer. Next day, the beads were washed five times with cold wash buffer (1% NP-40, 0.1% SDS, 1 mM DTT, 1 mM PMSF in PBS). Beads were dried with a syringe and needle and SDS sample buffer was added for subsequent western blot analysis.

Constructs and transfections

Constitutively active MRTF-A (ΔNMRTF-A), dominant negative MRTF-A (DN MRTF-A: ΔN1B1 and ΔNΔC) and MRTF-A–SRF reporter constructs have been previously characterised (Leitner et al., 2011). Constitutively active myc–mDia1 expression construct (myc-mDia1 FH1FH2) was amplified from an existing plasmid with forward primer 5′-gccaagaatgaaatggcttc-3′ and reverse 5′-tgcagagcttctagaagact, then the PCR product cloned into the pCRII-TOPO vector and sequenced. The integrin αV–mCherry and integrin β1–mCherry were generated in our laboratory (MPI Biochemistry, Martinsried). The knockdown constructs for stable knockdown of human ISG15 were purchased from Sigma and the UBP43 overexpression construct was obtained from Addgene. All transfections were carried out with Lipofectamine 2000 (Invitrogen through Life Technologies) according to the manufacturer's instructions.

Immunoblot detection of conjugated ISG15

Cells were incubated for 20 min with 50 µM of N-ethylmaleimide (NEM) and lysed on ice in RIPA buffer supplemented with 25 mM NEM and protease and phosphatase inhibitors. Protein concentration was measured by Bradford assay, samples were boiled for 5 min in Laemmli buffer containing 2% 2-mercaptoethanol.

MRTF-A–SRF luciferase reporter assay

Cells were plated on fibronectin coated 12-well plates (6.0×10^5 cells per well) before transient transfection with 0.5 µg of MRTF-A–SRF reporter (p3DA.luc) (Sotiropoulos et al., 1999), indicated expression plasmid and 25 ng thymidine-kinase-driven *Renilla* luciferase (Promega) for normalization of transfection efficiency. The total amount of transfected plasmid DNA was kept constant at 1.5 µg per well by using pEGFP-C1 expression vector (Clontech). After 24 h luciferase activity was analysed with a Dual Luciferase reporter assay kit (Promega) using a GloMax® Microplate Luminometer (Promega). Jasplakinolide (100 nM, #420107-50UG from Merck Millipore) and Latrunculin A (500 nM, L5163 from Sigma) treatment was initiated 3 h prior to cell lysis.

Micropatterning

Micropatterns were generated on PEG-coated glass coverslips with deep-ultraviolet lithography (Azioune et al., 2010). Glass coverslips were incubated in a 1 mM solution of a linear PEG, CH_3–$(O$–CH_2–$CH_2)_{43}$–NH–CO–NH–CH_2–CH_2–CH_2–$Si(OEt)_3$ in dry toluene for 20 h at 80°C under a nitrogen atmosphere. The substrates were removed, rinsed intensively with ethyl acetate, methanol and water, and dried with nitrogen. A PEGylated glass coverslip and a chromium-coated quartz photomask (ML&C, Jena) were immobilised with vacuum onto a mask holder, which was immediately exposed to deep ultraviolet light using a low pressure mercury lamp (NIQ 60/35 XL longlife lamp, quartz tube, 60 W from Heraeus Noblelight) at 5 cm distance for 7 min. The patterned substrates were subsequently incubated overnight with 100 µl of fibronectin (20 µg ml^{-1} in PBS) at 4°C and washed once with PBS.

FACS analysis

For FACS analysis suspension of fibroblasts was incubated for 1 h with primary antibodies on ice and then washed twice with FCS-PBS (3 mM EDTA, 2% FCS in PBS). Cell viability was assessed by propidium iodide staining. FACS analysis was carried out using a FACSCalibur Cytometer (BD Biosciences) and cell sorting with an AriaFACSII high-speed sorter (BD Biosciences), both equipped with FACS DiVa software (BD Biosciences). Purity of sorted cells was determined by post-sort FACS analysis and typically exceeded 95%. Data analysis was conducted using the FlowJo program (Version 9.4.10).

Quantitative real-time PCR

Total RNA from cells was extracted with RNeasy Mini extraction kit (Qiagen) following manufacturer's instructions. cDNA was prepared with an iScript cDNA Synthesis Kit (Bio-Rad). Real-time PCR was performed with an iCycler (Bio-Rad). Each sample was measured in triplicate and the values were normalised to *gapdh* levels. PCR primers are listed in Table S1.

Interferon ELISA

Cells were plated on fibronectin-coated tissue culture dishes for three days and the cell supernatant was analysed. To induce interferon production, cells were transfected with 100 µg/ml Poly(I:C). ELISA for interferon α and interferon β secretion was performed with the VeriKine™ Mouse IFN-α and Mouse IFN-β ELISA kits (PBL Interferon Source, product #42120 and #42400) according to manufacturer's instructions.

Trans-well migration assay

Invasion assay (Merck Millipore QCM™ Boyden chamber, 8 µm pore size) was performed according to manufacturer's instructions. MCF-7, MDA-MB-468 and MDA-MB-231 cells were seeded into polycarbonate trans-wells at a density of 3×10^4 cells and in a volume of 300 µl medium. Migration occurred for 12 h from serum-free medium towards medium with 10% FCS. After removing the non-migrating cells and staining the transmigrated cells with Phalloidin-TRITC and DAPI, micrographs were taken at 200× magnification. For each condition, cell migration was deduced by counting DAPI+ cell nuclei within 10 random regions on the trans-well membrane.

Chromatin immunoprecipitations (ChIP)

For all ChIP experiments, pKO-αV,β1 cells were used. Cross-linking, nuclei preparation and nuclease digestion of chromatin was performed according to manufacturer's instructions [SimpleCHIP Enzymatic Chromatin IP Kit (Magnetic Beads), #9003, Cell Signaling Technology]. Then, 500 µl of chromatin was incubated overnight at 4°C with 10 µl anti-SRF antibodies (#5147; Cell Signaling Technology) or 30 µl anti-MRTF-A rabbit serum (#79, our laboratory). After washing the immunoprecipitated chromatin, the DNA–protein complexes were eluted with the ChIP elution buffer.

Crosslinks were reversed overnight at 65°C, and DNA was purified using columns provided in the kit. Quantification was done by quantitative real-time PCR and is shown as the percentage of input chromatin. Gene-specific primers for amplification of immunoprecipitated DNA are listed in Table S1. Primers for *gapdh* and *srf* loci were published previously (Vartiainen et al., 2007).

RNA interference

Cells were infected with retroviral 29mer shISG15 expression constructs purchased from Sigma (#TG502956). Puromycin selection was used to select for cells carrying integrations.

Kaplan–Meier analysis of gene expression microarray

To analyse the prognostic value of *integrin αV*, *integrin β1* and *ISG15* mRNA expression levels the Kaplan–Meier plotter was used (http://kmplot.com/analysis/; Gyorffy et al., 2010). The patient samples were split into two groups according to various quantile expressions of the proposed biomarker (low and high expression). The two patient cohorts were compared by a Kaplan–Meier survival plot, and the hazard ratio with 95% confidence intervals and logrank *P*-value were calculated.

Statistics

Data are represented as the mean±s.e.m. of at least three independent experiments. Unless otherwise indicated, statistical significance was determined using unpaired two-tailed Student's *t*-test.

Acknowledgements

We thank Dr Julien Polleux for help with micropattern generation and Dr Assa Yeroslaviz for supporting the analyses of survival rates of breast cancer patients.

Competing interests

The authors declare no competing or financial interests.

Author contributions

R.F., M.-R.H., M.J. and G.P.C. designed the experiments; M.-R.H., M.J., G.P.C. and E.R. performed experiments; G.P. and C.K. provided important reagents and analytical tools; R.F., M.-R.H., M.J., G.P.C., E.R. analysed data; R.F. wrote the manuscript; all authors read the manuscript.

Funding

M.-R.H. was a fellow of the Boehringer Ingelheim Fonds. This work was supported by the European Research Council [ERC Grant Agreement no. 322652]; German Funding Agency [SFB 863]; and the Max Planck Society.

Supplementary information

Supplementary information available online at
http://jcs.biologists.org/lookup/suppl/doi:10.1242/jcs.177592/-/DC1

References

Azioune, A., Carpi, N., Tseng, Q., Théry, M. and Piel, M. (2010). Protein micropatterns: a direct printing protocol using deep UVs. *Methods Cell Biol.* **97**, 133-146.

Balza, R. O., Jr and Misra, R. P. (2006). Role of the serum response factor in regulating contractile apparatus gene expression and sarcomeric integrity in cardiomyocytes. *J. Biol. Chem.* **281**, 6498-6510.

Bishop, A. L. and Hall, A. (2000). Rho GTPases and their effector proteins. *Biochem. J.* **348**, 241-255.

Busche, S., Descot, A., Julien, S., Genth, H. and Posern, G. (2008). Epithelial cell-cell contacts regulate SRF-mediated transcription via Rac-actin-MAL signalling. *J. Cell Sci.* **121**, 1025-1035.

Connelly, J. T., Gautrot, J. E., Trappmann, B., Tan, D. W.-M., Donati, G., Huck, W. T. S. and Watt, F. M. (2010). Actin and serum response factor transduce physical cues from the microenvironment to regulate epidermal stem cell fate decisions. *Nat. Cell Biol.* **12**, 711-718.

Cooper, S. J., Trinklein, N. D., Nguyen, L. and Myers, R. M. (2007). Serum response factor binding sites differ in three human cell types. *Genome Res.* **17**, 136-144.

Danen, E. H. J., Sonneveld, P., Brakebusch, C., Fässler, R. and Sonnenberg, A. (2002). The fibronectin-binding integrins alpha5beta1 and alphavbeta3 differentially modulate RhoA-GTP loading, organization of cell matrix adhesions, and fibronectin fibrillogenesis. *J. Cell Biol.* **159**, 1071-1086.

Desai, S. D., Haas, A. L., Wood, L. M., Tsai, Y.-C., Pestka, S., Rubin, E. H., Saleem, A., Nur-E-Kamal, A. and Liu, L. F. (2006). Elevated expression of ISG15 in tumor cells interferes with the ubiquitin/26S proteasome pathway. *Cancer Res.* **66**, 921-928.

Desai, S. D., Reed, R. E., Burks, J., Wood, L. M., Pullikuth, A. K., Haas, A. L., Liu, L. F., Breslin, J. W., Meiners, S. and Sankar, S. (2012). ISG15 disrupts cytoskeletal architecture and promotes motility in human breast cancer cells. *Exp. Biol. Med.* **237**, 38-49.

Descot, A., Hoffmann, R., Shaposhnikov, D., Reschke, M., Ullrich, A. and Posern, G. (2009). Negative regulation of the EGFR-MAPK cascade by actin-MAL-mediated Mig6/Errfi-1 induction. *Mol. Cell* **35**, 291-304.

Durfee, L. A., Lyon, N., Seo, K. and Huibregtse, J. M. (2010). The ISG15 conjugation system broadly targets newly synthesized proteins: implications for the antiviral function of ISG15. *Mol. Cell* **38**, 722-732.

Esnault, C., Stewart, A., Gualdrini, F., East, P., Horswell, S., Matthews, N. and Treisman, R. (2014). Rho-actin signaling to the MRTF coactivators dominates the immediate transcriptional response to serum in fibroblasts. *Genes Dev.* **28**, 943-958.

Farrell, P. J., Broeze, R. J. and Lengyel, P. (1979). Accumulation of an mRNA and protein in interferon-treated Ehrlich ascites tumour cells. *Nature* **279**, 523-525.

Gyorffy, B., Lanczky, A., Eklund, A. C., Denkert, C., Budczies, J., Li, Q. and Szallasi, Z. (2010). An online survival analysis tool to rapidly assess the effect of 22,277 genes on breast cancer prognosis using microarray data of 1,809 patients. *Breast Cancer Res. Treatment* **123**, 725-731.

Haas, A. L., Ahrens, P., Bright, P. M. and Ankel, H. (1987). Interferon induces a 15-kilodalton protein exhibiting marked homology to ubiquitin. *J. Biol. Chem.* **262**, 11315-11323.

Hall, A. (2012). Rho family GTPases. *Biochem. Soc. Trans.* **40**, 1378-1382.

Han, S.-Y., Kim, S.-H. and Heasley, L. E. (2002). Differential gene regulation by specific gain-of-function JNK1 proteins expressed in Swiss 3T3 fibroblasts. *J. Biol. Chem.* **277**, 47167-47174.

Hermeking, H., Lengauer, C., Polyak, K., He, T.-C., Zhang, L., Thiagalingam, S., Kinzler, K. W. and Vogelstein, B. (1997). 14-3-3 sigma is a p53-regulated inhibitor of G2/M progression. *Mol. Cell* **1**, 3-11.

Hood, J. D. and Cheresh, D. A. (2002). Role of integrins in cell invasion and migration. *Nat. Rev. Cancer* **2**, 91-100.

Hoshino, D., Branch, K. M. and Weaver, A. M. (2013). Signaling inputs to invadopodia and podosomes. *J. Cell Sci.* **126**, 2979-2989.

Hu, Q., Guo, C., Li, Y., Aronow, B. J. and Zhang, J. (2011). LMO7 mediates cell-specific activation of the Rho-myocardin-related transcription factor-serum response factor pathway and plays an important role in breast cancer cell migration. *Mol. Cell. Biol.* **31**, 3223-3240.

Hynes, R. O. (2002). Integrins: bidirectional, allosteric signaling machines. *Cell* **110**, 673-687.

Jeon, Y. J., Choi, J. S., Lee, J. Y., Yu, K. R., Kim, S. M., Ka, S. H., Oh, K. H., Kim, K. I., Zhang, D.-E., Bang, O. S. et al. (2009). ISG15 modification of filamin B negatively regulates the type I interferon-induced JNK signalling pathway. *EMBO Rep.* **10**, 374-380.

Kerscher, O., Felberbaum, R. and Hochstrasser, M. (2006). Modification of proteins by ubiquitin and ubiquitin-like proteins. *Annu. Rev. Cell Dev. Biol.* **22**, 159-180.

Kressner, C., Nollau, P., Grosse, R. and Brandt, D. T. (2013). Functional interaction of SCAI with the SWI/SNF complex for transcription and tumor cell invasion. *PLoS ONE* **8**, e69947.

Legate, K. R., Wickstrom, S. A. and Fassler, R. (2009). Genetic and cell biological analysis of integrin outside-in signaling. *Genes Dev.* **23**, 397-418.

Leitner, L., Shaposhnikov, D., Mengel, A., Descot, A., Julien, S., Hoffmann, R. and Posern, G. (2011). MAL/MRTF-A controls migration of non-invasive cells by upregulation of cytoskeleton-associated proteins. *J. Cell Sci.* **124**, 4318-4331.

Lenschow, D. J., Giannakopoulos, N. V., Gunn, L. J., Johnston, C., O'Guin, A. K., Schmidt, R. E., Levine, B. and Virgin, H. W.IV. (2005). Identification of interferon-stimulated gene 15 as an antiviral molecule during Sindbis virus infection in vivo. *J. Virol.* **79**, 13974-13983.

Liu, M., Li, X.-L. and Hassel, B. A. (2003). Proteasomes modulate conjugation to the ubiquitin-like protein, ISG15. *J. Biol. Chem.* **278**, 1594-1602.

Lock, C., Hermans, G., Pedotti, R., Brendolan, A., Schadt, E., Garren, H., Langer-Gould, A., Strober, S., Cannella, B., Allard, J. et al. (2002). Gene-microarray analysis of multiple sclerosis lesions yields new targets validated in autoimmune encephalomyelitis. *Nat. Med.* **8**, 500-508.

Loeb, K. R. and Haas, A. L. (1992). The interferon-inducible 15-kDa ubiquitin homolog conjugates to intracellular proteins. *J. Biol. Chem.* **267**, 7806-7813.

Malakhov, M. P., Malakhova, O. A., Kim, K. I., Ritchie, K. J. and Zhang, D.-E. (2002). UBP43 (USP18) specifically removes ISG15 from conjugated proteins. *J. Biol. Chem.* **277**, 9976-9981.

Malakhova, O. A. and Zhang, D.-E. (2008). ISG15 inhibits Nedd4 ubiquitin E3 activity and enhances the innate antiviral response. *J. Biol. Chem.* **283**, 8783-8787.

Medjkane, S., Perez-Sanchez, C., Gaggioli, C., Sahai, E. and Treisman, R. (2009). Myocardin-related transcription factors and SRF are required for cytoskeletal dynamics and experimental metastasis. *Nat. Cell Biol.* **11**, 257-268.

Miralles, F., Posern, G., Zaromytidou, A.-I. and Treisman, R. (2003). Actin dynamics control SRF activity by regulation of its coactivator MAL. *Cell* **113**, 329-342.
Morales, D. J. and Lenschow, D. J. (2013). The antiviral activities of ISG15. *J. Mol. Biol.* **425**, 4995-5008.
Murphy, D. A. and Courtneidge, S. A. (2011). The 'ins' and 'outs' of podosomes and invadopodia: characteristics, formation and function. *Nat. Rev. Mol. Cell Biol.* **12**, 413-426.
Neve, R. M., Chin, K., Fridlyand, J., Yeh, J., Baehner, F. L., Fevr, T., Clark, L., Bayani, N., Coppe, J.-P., Tong, F. et al. (2006). A collection of breast cancer cell lines for the study of functionally distinct cancer subtypes. *Cancer Cell* **10**, 515-527.
Okumura, F., Zou, W. and Zhang, D.-E. (2007). ISG15 modification of the eIF4E cognate 4EHP enhances cap structure-binding activity of 4EHP. *Genes Dev.* **21**, 255-260.
Okumura, A., Pitha, P. M. and Harty, R. N. (2008). ISG15 inhibits Ebola VP40 VLP budding in an L-domain-dependent manner by blocking Nedd4 ligase activity. *Proc. Natl. Acad. Sci. USA* **105**, 3974-3979.
Okumura, F., Okumura, A. J., Uematsu, K., Hatakeyama, S., Zhang, D.-E. and Kamura, T. (2013). Activation of double-stranded RNA-activated protein kinase (PKR) by interferon-stimulated gene 15 (ISG15) modification down-regulates protein translation. *J. Biol. Chem.* **288**, 2839-2847.
Olson, E. N. and Nordheim, A. (2010). Linking actin dynamics and gene transcription to drive cellular motile functions. *Nat. Rev. Mol. Cell Biol.* **11**, 353-365.
Philippar, U., Schratt, G., Dieterich, C., Müller, J. M., Galgóczy, P., Engel, F. B., Keating, M. T., Gertler, F., Schüle, R., Vingron, M. et al. (2004). The SRF target gene Fhl2 antagonizes RhoA/MAL-dependent activation of SRF. *Mol. Cell* **16**, 867-880.
Plessner, M., Melak, M., Chinchilla, P., Baarlink, C. and Grosse, R. (2015). Nuclear F-actin formation and reorganization upon cell spreading. *J. Biol. Chem.* **290**, 11209-11216.
Posern, G. and Treisman, R. (2006). Actin' together: serum response factor, its cofactors and the link to signal transduction. *Trends Cell Biol.* **16**, 588-596.
Schiller, H. B., Hermann, M.-R., Polleux, J., Vignaud, T., Zanivan, S., Friedel, C. C., Sun, Z., Raducanu, A., Gottschalk, K.-E., Théry, M. et al. (2013). beta1- and alphav-class integrins cooperate to regulate myosin II during rigidity sensing of fibronectin-based microenvironments. *Nat. Cell Biol.* **15**, 625-636.
Selvaraj, A. and Prywes, R. (2004). Expression profiling of serum inducible genes identifies a subset of SRF target genes that are MKL dependent. *BMC Mol. Biol.* **5**, 13.
Small, J.-V., Rottner, K., Hahne, P. and Anderson, K. I. (1999). Visualising the actin cytoskeleton. *Microsc. Res. Tech.* **47**, 3-17.
Sotiropoulos, A., Gineitis, D., Copeland, J. and Treisman, R. (1999). Signal-regulated activation of serum response factor is mediated by changes in actin dynamics. *Cell* **98**, 159-169.
Sun, Q., Chen, G., Streb, J. W., Long, X., Yang, Y., Stoeckert, C. J., Jr and Miano, J. M. (2006). Defining the mammalian CArGome. *Genome Res.* **16**, 197-207.
van der Veen, A. G. and Ploegh, H. L. (2012). Ubiquitin-like proteins. *Annu. Rev. Biochem.* **81**, 323-357.
Vartiainen, M. K., Guettler, S., Larijani, B. and Treisman, R. (2007). Nuclear actin regulates dynamic subcellular localization and activity of the SRF cofactor MAL. *Science* **316**, 1749-1752.
Vicente-Manzanares, M., Choi, C. K. and Horwitz, A. R. (2009). Integrins in cell migration–the actin connection. *J. Cell Sci.* **122**, 199-206.
Winograd-Katz, S. E., Fässler, R., Geiger, B. and Legate, K. R. (2014). The integrin adhesome: from genes and proteins to human disease. *Nat. Rev. Mol. Cell Biol.* **15**, 273-288.
Yuan, W. and Krug, R. M. (2001). Influenza B virus NS1 protein inhibits conjugation of the interferon (IFN)-induced ubiquitin-like ISG15 protein. *EMBO J.* **20**, 362-371.
Zhang, S. X., Garcia-Gras, E., Wycuff, D. R., Marriot, S. J., Kadeer, N., Yu, W., Olson, E. N., Garry, D. J., Parmacek, M. S. and Schwartz, R. J. (2005). Identification of direct serum-response factor gene targets during Me2SO-induced P19 cardiac cell differentiation. *J. Biol. Chem.* **280**, 19115-19126.